Author/s:
Tran, H;Thai, HT;Ngo, T;Uy, B;Li, D;Mo, J

Title:
Nonlinear inelastic simulation of high-rise buildings with innovative composite coupling shear walls and CFST columns

Date:
2021-09-01

Citation:
Tran, H., Thai, H. T., Ngo, T., Uy, B., Li, D. & Mo, J. (2021). Nonlinear inelastic simulation of high-rise buildings with innovative composite coupling shear walls and CFST columns. Structural Design of Tall and Special Buildings, 30 (13), https://doi.org/10.1002/tal.1883.

Persistent Link:
https://hdl.handle.net/11343/298696

Thai Huu-Tai (Orcid ID: 0000-0002-4461-9548)

Nonlinear inelastic simulation of high-rise buildings with innovative composite coupling shear walls and CFST columns

Hau Tran[a], Huu-Tai Thai[a,*], Tuan Ngo[a], Brian Uy[b], Dongxu Li[b], Jun Mo[b]

[a] Department of Infrastructure Engineering, The University of Melbourne, Parkville, VIC 3010, Australia

[b] School of Civil Engineering, The University of Sydney, Sydney, NSW 2006, Australia

Abstract

This paper investigates the behaviour of high-rise composite buildings with composite shear walls and concrete-filled steel tubular (CFST) columns using a numerical model in OpenSees. In the model, the geometric and material nonlinearity of structural elements are captured by utilizing a fibre force-based beam-column elements with rigorously modified material stress-strain relationships. Besides, the confining effect of the concrete core, the semi-rigid connections and the coupling effect of composite shear walls are carefully taken into consideration. Finally, the case study of a 42-storey composite building is conducted using the proposed model to provide a thorough understanding about the behaviour of this kind of building. It shows that this innovative building has high loading capacity and significantly reduces the dimension of structural members (up to 50%) compared with the conventional RC building at the same loading capacity. Through the validation with test data, the suggested constitutive laws have shown the simplicity and high accuracy since the value of model error is only around 7%. In addition, the simulation results also indicate that the model can capture well the nonlinear behaviour of tested specimens, especially, the failure and the formation of

* Corresponding author. Tel.: +61 3 8344 6196
E-mail address: tai.thai@unimelb.edu.au (H.T. Thai)

This is the author manuscript accepted for publication and has undergone full peer review but has not been through the copyediting, typesetting, pagination and proofreading process, which may lead to differences between this version and the Version of Record. Please cite this article as doi: 10.1002/tal.1883

plastic hinges of coupling composite shear walls implicitly.

Keywords: CFST column; coupling composite shear wall; composite high-rise building; OpenSees; material model; semi-rigid connection

1. Introduction

Concrete structures that comprise of structural steel and concrete have been increasingly used in recent years due to its excellent structural performance and construction benefits. One of the most efficient approaches in steel-concrete composite structures is in the form of concrete-filled steel tubes (i.e., CFST columns) or steel faces (i.e., composite shear walls) which display better strength and ductility characteristics [1]. Due to the novelty and efficiency of this approach, numerous studies on isolated structural elements such as CFST columns and concrete-filled double skin steel shear walls have been conducted to assess the behaviour of concrete-filled steel tubular elements and structural systems [2-8]. Thai et al. [6] and Tao et al. [5] developed 3D numerical models in ABAQUS for the simulation of square and circular CFST columns, which are able to capture the performance of high strength materials. Uy [9-13] investigated the local and post-local buckling effect of rectangular CFST columns with fabricated steel tubes. Sakino et al. [14] and Fujimoto et al. [15] carried out experiments on a large number of specimens to propose a mathematical model that can precisely predict the force characteristic of CFST columns and the simultaneous interaction between in-filled concrete and the steel tube. Liang and Fragomeni [16] proposed constitutive models that were able to capture the characteristics of both normal and high strength concrete confined by either normal or high strength circular steel tubes, which was then implemented in fibre models to simulate nonlinear inelastic behaviour of CFST short columns under axial load. Recently, Thai et al. [17]

collected a comprehensive test database of CFST columns with over 3,100 specimens to evaluate the applicability of current codes of practice for the design of CFST columns with material and slenderness ratios beyond the code limits. Isolated composite shear walls and coupling composite shear walls also attract significant research attention [18-20]. In addition, many studies on the performance of composite frames [2, 7] and composite buildings [21-23] have also been conducted. Even though extensive studies have been carried out and a large range of knowledge on CFST members has been provided, none of the aforementioned research has focused on the behaviour of high-rise buildings constructed from CFST columns and composite shear walls. As a result, there is no available model for the analysis of such buildings.

Regarding the simulation method of studies mentioned, the nonlinear response of structural members can be captured by different types of elements in finite element software or developed source codes. In particular, the best approach for the numerical analysis is based on solid and shell elements to build the simulation model. In this method, the physical shapes of structural components can be perfectly reflected with detailed modelling of bolted connections between beams and columns or the shear studs between concrete slabs and steel beams [24]. Therefore, the semi-rigid behaviour and the shear behaviour at these locations are captured simultaneously. Although this form of model can provide highly reliable results, it creates extraordinary pressure on the requirements of the computational system and required computational time. As a result, this method is only limited to meso-scale models of the isolated members such as CFST columns, composite shear walls or complex composite joints [5, 19, 24]. However, for macro-scale models like high-rise buildings, it is obviously unsuitable and impractical due to computational cost. Another option is the use of computationally efficient 1D models like beam "line" elements with the fibre hinge concept for capturing the inelastic behaviour of materials. This approach has been implemented in many studies when all structural components such as shear walls, beams and columns can be simulated by line elements to simplify the simulation procedure and significantly reduce the calculation time [25-28]. Moreover, the use of 1D beam line models makes the implementation of semi-rigid connections much easier by simply adding the moment-rotation relationship obtained from experiments.

Although there have been numerous studies investigating the behaviour of CFST structural members and composite frames or composite buildings as mentioned above, the analysis on high-rise composite buildings constructed from CFST columns and coupling composite shear walls has not been found. In this paper, the behaviour of innovative high-rise composite buildings with innovative coupling concrete-filled double steel skin shear walls and CFST columns is investigated by the proposed numerical model using the fibre force-based beam element in OpenSees. In the model, all sources of nonlinearities from geometry, material and semi-rigid connection are carefully considered. The modelling technique of each structural component, especially coupling composite shear walls, is presented and verified with the experimental results to show the simplicity and accuracy of the proposed model. Moreover, the extensive parametric study is conducted to provide deep understanding about this new kind of building.

2. Finite element model

2.1 Force-based fibre beam-column element

There are two types of the fibre beam-column element available in OpenSees including displacement-based element (*dispBeamColumn*) and force-based element (*forceBeamColumn*).

Unlike concentrated plasticity model, the fibre model can capture the spread of plasticity along the element [29]. The difference between the *dispBeamColumn* element and *forceBeamColumn* element was presented by Terzic [30]. It is suggested that the *forceBeamColumn* element is the most suitable element for modelling reinforced concrete and steel-concrete composite structures due to its computational efficiency while it can precisely predict the results with only 1 element per structural member (Fig. 1). Therefore, the *forceBeamColumn* element is adopted in this study.

In the fibre model, the inelastic behaviour will be captured by monitoring the uniaxial stress-strain relationship of each fibre on the cross sections located at the integration points along the member length [29]. Hence, the choice of an appropriate material model for steel and concrete in composite members is of paramount importance. In this paper, *concrete02* and *reinforcingSteel* material are utilized. However, it should be noted that the constitutive law for hysteretic behaviour of both steel and concrete is not presented herein because they are already integrated in the two mentioned materials, and the authors did not make any modification.

2.1.1 Material model for concrete

The uniaxial stress-strain relationships of unconfined concrete and confined concrete with both compression and tension behaviour are illustrated in Fig. 2a. For unconfined concrete in compression, this paper utilizes a simple model proposed by Kent and Park [31] in which the stress-strain of concrete is reflected by Eq. (1). This model includes three phases with nonlinear behaviour at pre-peak stage and simplified linear behaviour at post-peak stages. This model is integrated in *Concrete02* in OpenSees and it can be implemented by inputting parameters such as f_c, ε_o, f_{cu} and ε_{cu} that are explicitly explained following:

$$\sigma = \begin{cases} E\varepsilon - \dfrac{E}{2\varepsilon_o}\varepsilon^2 & for\ \varepsilon \le \varepsilon_o \\ f_c - \dfrac{f_c - 0.2f_c}{\varepsilon_{cu} - \varepsilon_o}(\varepsilon - \varepsilon_o) & for\ \varepsilon_o < \varepsilon \le \varepsilon_{cu} \\ 0.2 f_{cu} & for\ \varepsilon > \varepsilon_{cu} \end{cases} \tag{1}$$

in which σ (MPa) and ε are the concrete stress and strain, respectively; f_c (MPa) is the compressive strength of concrete which can be simply taken directly from the concrete cylinder compressive strength or calculated from the cubic compressive strength (0.8 f_{cubic}); E (MPa) is the elastic modulus of concrete that can be found based on the instruction of ACI318-14 as $4700\sqrt{f_c}$ [32]; ε_o is the strain corresponding to the concrete compressive strength taken as $2f_c / E$, whilst the ultimate compressive strain can be taken as $\varepsilon_{cu} = 4\varepsilon_o$ [33] and the corresponding compressive stress is $f_{cu} = 0.2f_c$. The hysteretic rules are also included in *Concrete02*[34].

Since concrete is filled inside the steel tube, the confinement from the steel tube contributes to the increase in concrete compressive strength and ductility as reported in many studies [6, 14-16, 35]. In this research, the stress-strain relationship of confined concrete is also based on Kent and Park's model [31], but it's compressive strength is calculated based on the equation given by Mander et al. [36] as:

$$f_{cc} = f_c + k_1 f_{rp} \tag{2}$$

where f_{rp} (MPa) is the confining stress caused by steel tube on concrete core, which is strongly dependent on the shape of CFST columns; k_1 varies from 4.0 to 7.0 as observed from the experiment [37-38] and the value 4.0 is recommended. The strain corresponding to the strength of confined concrete f_{cc} is suggested to be $\varepsilon_{cc} = 2f_{cc} / \left(4700\sqrt{f_{cc}}\right)$ in this study, and it will be calibrated later by numerous simulations of CFST members.

For square CFST columns, the formula given by Susantha et al. [39] is adopted to calculate the value of confining stress f_{rp}:

$$f_{rp} = -6.5R\frac{f_c^{1.46}}{f_y} + 0.22f_c^{1.03} \tag{3}$$

in which *R* is the width-to-thickness ratio parameter that can be determined as:

$$R = \frac{b}{t}\sqrt{\frac{12\left(1-\upsilon_s^2\right)}{4\pi^2}}\sqrt{\frac{f_y}{E_s}} \tag{4}$$

where *b* and *t* are the width and thickness of the steel tube, respectively; E_s is the elastic modulus of the steel tube and υ_s is the steel Poisson's ratio.

For circular sections, the confined effect due to the hoop stress in the steel tube can be observed more clearly due to the significant increase in compressive strength of concrete as presented in some studies [14-15]. Therefore, the confining pressure is entirely different from that of square sections, and it can be captured accurately by the equation proposed by [16]:

$$f_{rp} = \begin{cases} 0.7\left(\upsilon_e - \upsilon_s\right)\dfrac{2t}{D-2t}f_y & for\ \dfrac{D}{t} \le 47 \\ \left(0.006241 - 0.0000357\dfrac{D}{t}\right)f_y & for\ 47 < \dfrac{D}{t} \le 150 \end{cases} \tag{5}$$

where *D* and *t* are the diameter and thickness of the steel tube, respectively; υ_e is Poisson's ratio of the steel tube with in-filled concrete defined by Tang et al. [40] as:

$$\upsilon_e = 0.2312 + 0.3582\upsilon_e' - 0.1524\left(\frac{f_c}{f_y}\right) + 4.843\upsilon_e'\left(\frac{f_c}{f_y}\right) - 9.169\left(\frac{f_c}{f_y}\right)^2 \tag{6}$$

$$\upsilon_e' = 0.881\times10^{-6}\left(\frac{D}{t}\right)^3 - 2.58\times10^{-4}\left(\frac{D}{t}\right)^2 + 1.953\times10^{-2}\left(\frac{D}{t}\right) + 0.4011 \tag{7}$$

The post-peak behaviour of confined concrete in circular sections is defined by ultimate strain $\varepsilon_{ccu} = 4\varepsilon_{cc}$ and corresponding compressive stress $f_{ccu} = f_{cc} - Z(\varepsilon_{ccu} - \varepsilon_{cc})$. The value of Z is given by Susantha et al. [39] as:

$$Z = \begin{cases} 0 & for\ R_t\left(f_c / f_y\right) \le 0.006 \\ 1.0\times10^5 R_t \dfrac{f_c}{f_y} - 600 & for\ R_t\left(f_c / f_y\right) \ge 0.006\ and\ f_y \le 283MPa \\ 1.0\times10^6 R_t \dfrac{f_c}{f_y} - 6000 & for\ R_t\left(f_c / f_y\right) \ge 0.006\ and\ f_y \ge 336MPa \\ \left(\dfrac{f_y}{283}\right)^{13.4}\left[1.0\times10^5 R_t \dfrac{f_c}{f_y} - 600\right] & for\ R_t\left(f_c / f_y\right) \ge 0.006\ and\ 283 \le f_y \le 336MPa \end{cases} \tag{8}$$

where R_t is the radius-to-thickness ratio defined as:

$$R_t = \sqrt{3\left(1-\upsilon^2\right)}\frac{f_y}{E_s}\frac{D}{2t} \tag{9}$$

The behaviour of concrete in tension is simply considered bilinear as depicted in Fig. 2a. The tensile strength of concrete is taken as $f_t = 1.4\left(f_c / 10\right)^{2/3}$ following CEB-FIB 1990 [41]. However, concrete in tension shows less influence on the behaviour of CFST members.

2.1.2 Material model for steel

A variety of steel models can be used to represent the elastic-plastic behaviour of steel. Traditional models for steel are based on the engineering stress-strain relationship that underestimates the steel strength in tension and overestimates the steel strength in compression.

In this study, the steel model proposed by Kunnath et al. [42] is applied by using the *ReinforcingSteel* material model in OpenSees (Fig. 2b). This model will automatically transfer an input engineering stress-strain relationship to a natural stress-strain relationship. In addition, the buckling phenomenon of the steel tube in compression is also taken into consideration in this material model by inputting the slenderness ratio that is suggested as the proportion of tie bars spacing and steel plate thickness in this study. Further details concerning the buckling model are given by Gomes and Appleton [43]. To use the *ReinforcingSteel* model, some key parameters need to be defined such as the steel yield strength f_y, the steel ultimate strength f_{su}, the initial elastic modulus E_s, the modulus at the initial strain hardening $E_{sh} = 0.02E_s$ [5], the strain corresponding to the initial strain hardening ε_{sh} and the strain corresponding to the ultimate strength ε_{su}. The values of ε_{sh} and ε_{su} are given by Tao et al. [5] as $\varepsilon_{sh} = 15 f_y / E_s$ and $\varepsilon_{su} = 100 f_y / E_s$.

2.2 Zero-length spring element for semi-rigid connections

The connections between composite beams to CFST columns and composite beams to composite shear walls play an important role in the load-carrying capacity and the stiffness of the composite buildings, especially when these structural components are connected by bolts. Traditionally, fully-rigid connections or pin connections are assumed, but they overestimate or underestimate the stiffness of joints. Therefore, to accurately model the behaviour of joints, the semi-rigid behaviour at the connections needs to be considered by means of the moment-rotation relationship that can be found by various methods such as Kishi-Chen three-parameter model [44], component method recommended in Eurocode [45-46] and experimental tests.

In this research, the semi-rigid connection is modelled by utilizing the zero-length element in OpenSees. The zero-length element has six degrees of freedom corresponding to translations and rotations in three axes. Hence, the semi-rigid behaviour can be captured by implementing moment-rotation curves into rotational springs around the investigated directions. Since the beam-column element is used for the simulation of all structural members, it is perfectly feasible to add zero-length elements at the shared nodes between columns, beams, and shear walls. In addition, the stiffness of each spring element can also be modified to represent the cases of fully rigid or pin connections. For the translational springs and out-of-plane rotational springs, their behaviour is considered fully rigid by assigning very large value of stiffness. The stiffness of rotational spring in the working plane is taken from experiment and Eurocode 3[45] as presented in part 3.6 and part 4.1 of the paper, respectively.

2.3 Modelling of CFST columns and steel – concrete composite beams

This study utilizes only beam-column elements to simulate CFST columns and composite beams. In this approach, both concrete and the steel of CFST columns and composite beams are incorporated into one beam-column element by using fibre sections in which concrete and steel are divided into numerous fibres as illustrated in Fig. 3. Therefore, the contact at the interface between concrete and steel tube or concrete slab and steel beam is considered fully rigid even though there is slip at these contact interactions. However, it has been found that the slip at the concrete-steel interface has little impact on the overall load-carrying capacity of large-scale structures, and thus it can be neglected [23]. For composite beam, the effective flange width of the concrete slab, unless mentioned otherwise, can be calculated using the instructions of EC2 [47] as:

$$b_{eff} = \sum b_{eff,i} + b_w \le b \quad (10)$$

$$b_{eff,i} = 0.2b_i + 0.1l_o \le 0.2l_o,\ \ and\ b_{eff,i} \le b_i \quad (11)$$

where b_w is the width of the beam; b is half of the total length of spans adjacent to the current beam; b_i is half of the length of each span adjacent to the current beam; and l_o is the distance between points of zero moment.

2.4 Modelling of isolated composite shear walls and coupling composite shear walls

The simulation of isolated shear walls is similar to those of CFST columns (Fig. 3), which is also based on the beam-column element with the aforementioned fibre sections. The model for coupling composite shear wall systems is shown in Fig. 4. Since the shear wall is modelled by the beam-column element located at the middle of its section, it cannot reflect physical dimension and the load-transferring mechanism of the shear wall. As a result, a rigid link element is utilized to represent the physical width of the shear wall based on the assumption that the shear wall section will remain plane after deformation. The rigid link element has infinite stiffness that enables it to transfer all initial deformations appearing at any position along the width of the shear wall due to external loads. Coupling beams are also modelled by beam-column elements connected to the shear wall through the rigid link elements at two ends by zero-length spring element with assigned force-deformation relationships of the beam-to-shear wall joints. Since the coupling beams mainly resist the shear force, their shear behaviour cannot be ignored. In this study, a bilinear shear force-shear deformation relationship is employed for the shear springs as depicted in Fig. 4. The initial shear stiffness of coupling beams $k_{b,i}$ in this study is suggested to be calculated based on the shear modulus of steel G_{sw}

and concrete G_c as:

$$k_{b,i} = \frac{G_{sw}A_{sw} + 0.01\alpha_s G_c A_c}{l_b} \tag{12}$$

where A_{sw} is steel area of the beam web; A_c is the concrete area of the coupling beam; l_b is the length of the beam segments; the coefficient 0.01 [25] is the ratio of the fully cracked shear modulus to the un-cracked shear modulus and α_s is the shape coefficient taken as 5/6 for rectangle section [25]. The shear resistance of the coupling beam is determined based on of AISC341-16 (section 5d) [48]:

$$V_{y,cb} = 1.1R_y V_p + 0.21\sqrt{R_c f_c} b_{wc} d_c \tag{13}$$

$$V_p = 0.6 f_y A_{sw} \tag{14}$$

in which R_y is the ratio of the expected yield stress to the specified minimum yield stress of steel; R_c is the factor that accounts for the expected strength of concrete taken as 1.5; b_{wc} is the width of the in-filled concrete, and d_c is the effective depth of the in-filled concrete.

In tall buildings, the height-to-width ratio of the shear wall is dramatically large. Therefore, the flexural behaviour will be dominant. However, the shear behaviour is also taken into consideration in this study by aggregating a shear section carrying the linear shear force-shear strain relationship into the fibre section (Fig. 4). The shear stiffness is calculated based on Eq. (12) as:

$$K_w = G_{sw}A_{sw} + 0.01\alpha_s G_c A_c \tag{15}$$

where G_{sw}, A_{sw}, α_s, G_c and A_c are same as those defined above.

3. Model verification

3.1 Composite beam

Nie and Cai [49] explored the influence of the shear slip on the deformation of steel-concrete composite beams by conducting experiments considering different types of loading condition. A simply supported beam from their test, namely SCB-3, is simulated to verify the proposed model. The compressive strength of concrete is 27.7 MPa and the yield strength of steel is 310 MPa. This beam is subjected to monotonic load at the middle of the beam.

Another continuous composite beam among specimens tested by Ansourian [50], namely CTB4, is modelled in this section. The concrete compressive strength and the steel yield strength are 34 MPa and 236 MPa, respectively. Since this beam has two spans subjected to static load applied at each span, hogging moment at the middle support and sagging moments at middle spans will appear. Hence, the accuracy of the models for concrete in tension and compression will be validated. The geometry of the two composite beams are illustrated Fig. 5.

Fig. 6 shows the comparison on the results from numerical simulation and those from the experiments tested by Nie and Cai [49] and Ansourian [50]. It can be seen that a good agreement between the results in terms of the initial stiffness and ultimate load-carrying capacity is obtained. The comparison results also reveal that the computational efficiency of the *forceBeamColumn* element when only one element per member is used in the modelling.

3.2 CFST column

In recent decades, a large number of both rectangular and circular CFST columns have been tested and collected by Thai et al. [17]. However, only typical specimens are used in this study to verify the accuracy of proposed model. The geometry and material properties of these specimens are presented in Table 1 in which *Rect.* and *Cir.* denote rectangular and circular sections, respectively; *B*, *D* and *t* are the width, diameter and thickness of the steel tube. Square CFST columns are also modelled and they are considered as special cases of rectangular columns with aspect ratio equal to 1.0. The investigated CFST columns are comprised of both highly ductile members and moderately ductile members with slenderness (*D/t*) varying significantly in a wide range from 18.8 to 125. In addition, the steel tubes of CFST columns considered in this paper include slender sections, non-compact sections and compact sections (see AISC360-16 [51] for the classification) made from both high strength steel and normal steel with the yield strength from 265.8 MPa to 853 MPa. The in-filled concrete has compressive strength from 25.4 MPa to 157 MPa. Hence, the beam element used in this study can be used to verify a wide range CFST columns with different configurations and material strengths.

Table 1 shows the comparison between the simulations and experimental results. As indicated in Table 1, the test-to-prediction ratios of the ultimate loads are relatively close to unity with the mean value of 0.99 and the standard deviation of 0.067, this evidently shows the favourable accuracy of the proposed model. A breakdown result of all specimens is also shown in Fig. 7, and it can be seen that the test-to-prediction ratios are within 10% for all specimens considered. The load-deflection behaviours of some typical specimens are also compared in Fig. 8 for rectangular columns and Fig. 9 for circular columns. It can be observed that the present fibre beam-column element can capture well both the initial stiffness and post-buckling behaviour of both rectangular and circular CFST columns.

3.3 Isolated composite shear wall

Although many experimental studies on concrete filled double steel skin shear walls have been found [8, 18-20, 52-53], very few of them considered shear walls with realistic dimensions. Therefore, only a limited number of specimens that are taken from the work of Eom et al. [52] and Varma et al. [20] are simulated to verify the proposed model. It should be noted that these shear walls have relatively large height-to-width ratio (from 2.97 to 6.67) implying that flexural failure will be their dominant failure mode. More details about the geometry and material properties of the shear walls are given in Fig. 10 and Table 2 in which h and w are the height and the width of shear walls, respectively, t is the thickness of shear walls and t_p is the thickness of steel face plates. In addition, specimens considered here have both rectangular sections and T-sections, and they are subjected to lateral loads or both lateral loads and axial loads.

Table 2 shows the comparison of the ultimate lateral loads obtained from experiment ($V_{u,exp}$) and simulation ($V_{u,cal}$). The values of mean and standard deviation of the test-to-prediction ratios $V_{u,exp}$/ $V_{u,cal}$ are 1.069 and 0.04, respectively, indicating that the difference in the load-carrying capacity between test and simulation is negligible. In Fig. 11, the lateral load-lateral displacement relationships of isolated shear walls are depicted. The initial stiffness, the ultimate load and the post-peak behaviour of these shear walls are captured relatively well, and a good agreement between test and simulation has been found.

3.4 Coupling composite shear wall

Two coupling composite shear walls namely DSCW4 with rectangular section and DSCW5 with T- section tested by Eom et al. [52] are simulated to verify the proposed model. In both two specimens, the coupling beams used to connect the composite shear walls are CFST beams which are welded to the edges of the shear walls. To avoid the fracture at the welded connections between the coupling beams and the shear walls in specimen DSCW5, additional cover steel plates have been used to strengthen these joints. More information about the geometry and material properties of these coupling composite shear walls can be found in Table 2 and Fig. 12.

The comparison between test and simulation of load-displacement curves of the composite coupling shear wall specimens subjected to cyclic loads is presented in Fig. 13. In the experiment, the shear wall DSCW4 failed because of concrete crushing, local buckling of plate and the fracture in coupling beams, the shear wall DSCW5 failed due to fracture in coupling beams. As can be seen in the figure, good agreement has been found between simulation and experiment in term of both loading capacity, loading and unloading procedure. This good correlation indicates that the proposed model can implicitly capture the failure of the two specimens quite well. Therefore, the proposed model is capable of predicting the response of shear walls and coupling shear walls subjected to lateral loads or both lateral loads and axial loads.

3.5 Composite frame with rigid connections

Udagawa and Mimura [54] conducted a pseudo dynamic test to explore the behaviour of the portal frames comprised of steel columns and steel-concrete composite beams. A specimen, namely CCE-5, in their experiment is simulated herein for model verification. The cube compressive strength of concrete is 22.6 MPa and the yield strength of steel is 335 MPa. The geometry of specimens is depicted in Fig. 14a. The comparison between test and simulation on the relationships between lateral force ($P/{}_sP_p$) and lateral displacement ($U/{}_sU_p$) of presented specimens is given in Fig. 14b with P and u being the lateral force and the displacement of composite frames, respectively. ${}_sP_p$ and ${}_sU_p$ are respectively normalization values of the lateral force and the displacement of steel frame, which are determined based on the assumption that moments at the ends of steel beams reach the full plastic moments. Through the comparison, good agreement between test and simulation has been observed as shown in Fig. 14b.

3.6 Composite frame with semi-rigid connections

Wang and Li [55] investigated the effect of semi-rigid connections on the behaviour of a two-storey two-bay composite frame subjected to an increasing gravity load up to failure. The frame includes steel-concrete composite beams (beams 1-4 in Fig. 15) linked to steel columns by means of bolted connections. The geometric dimension of the frame is given in Fig. 15. The cube compressive strength of concrete is 22.6 MPa and the yield strength of steel is 335 MPa. Since the behaviour of the bolted endplate beam-to-column connections is classified as semi-rigid, its behaviour needs to be included in the simulation. In this study, the zero-length spring element is used to model the connection between composite beams and steel columns. The moment-rotation behaviour of the connection is taken from the experimental study [55].

Fig. 16 shows the comparison of the load-deflection behaviours and bending moment distributions obtained from the simulation and experimental test. Both rigid and semi-rigid results are considered in this study to illustrate the effect of semi-rigid behaviour of the beam-to-column connection. The predictions with semi-rigid connections are very close to those of the test results, especially the initial stiffness and bending moment distribution. Whereas, the result obtained from the model with rigid connections shows a clear discrepancy with the experimental result indicating the significant effect of the semi-rigid behaviour of the connection on the global behaviour of the frame. Therefore, it should be considered in the analysis and design.

4. Case study of a 42-storey composite building

The configuration of the 42-storey composite building (Fig. 17a) considered in this study is referred from that of a 42-storey reinforced concrete (RC) building given in Refs. [56-57]. The residential RC building located in Los Angeles (USA) includes four basements and 42 stories with the total height of 141.8m above the ground. In this building, the RC core tube - perimeter frames system was utilized and they are connected by flat slab and main beams (as shown in the typical floor of the building in Fig. 17b). The dimension of the beams is 760x915 mm, the dimension of columns varies in the range from 900x900 mm to 1200x1200 mm and the thickness of the shear walls is around 600 mm and 450 mm with the compressive strength of concrete ranging from 34.5 MPa to 69 MPa. The building is subjected to both gravity load and inverted triangular lateral load along the X direction. This RC building is modelled in this study using the fibre beam-column element only. Particularly, the section of beams, columns and shear walls including both concrete and reinforcement along with their material properties are defined clearly using fiber-section, which then is assigned to the force based beam-column element in OpenSees. The beam-column element is located at the middle of the shear walls and the connection of these shear walls to beams or the connection between columns and beams are considered fully rigid. The rigid diaphragm is defined at each floor using rigidDiaphragm command in OpenSees. Since the basements of the building is not taken into account in the simulation[56], the fixed support is considered at the ground level of the building. In the study by Lu et al. [56], the RC building was simulated using both beam-column element (for beam and column members) and shell element (for shear walls). Therefore, a negligible discrepancy of the base shear force and lateral displacement behaviour obtained from the present model and

Lu et al. [56] has been found (Fig. 18).

In order to create the composite building used in this case study, this RC building is then modified by replacing RC sections of columns, beams and shear walls by corresponding steel-concrete composite sections based on the assumption that the load-carrying capacity of the composite building is equivalent to that of the RC building. In particular, the section of the composite beams was chosen to have the same moment capacity of the concrete beams. Since the seismic design is not considered in this study, the section dimension of CFST columns was selected to meet the requirements of moderately ductile members (section D1, AISC341-16[48]). The area of the steel plates in the section should account for at least 1% the total area of section of the shear walls[20], and the maximum spacing of tie bars meets the requirement of section H7.4b of AISC341-16[48]. After that, the push-over analysis is conducted and the dimensions of those sections are adjusted until the lateral loading capacity of the composite building equals to that of the concrete building. The dimensions of structural elements and material properties of the composite building are given in Table 3. The result of pushover analysis of the composite building is also shown in Fig. 18 in which the brittle failure occurred due to the sudden crushing of concrete in the composite sections. This phenomenon can be observed more clearly if the compressive strength of concrete is increased (Fig. 20a). By using the composite sections, the dimensions of structural elements can be decreased significantly. The cross-section of columns can be reduced by up to 50% from around 900x900mm (RC section) to 600x600mm (CFST section), whilst the cross-section of shear walls is reduced from around 600mm (RC section) to 350mm (composite section). From this validated model, an extensive parametric study is conducted to investigate the influence of a wide range of geometric and material parameters on the behaviour of the 42-storey composite building.

4.1 Effect of semi-rigid connection

In order to explore the effect of semi-rigid behaviour of connections on the behaviour of the composite high-rise building, various moment-rotation curves with different stiffness values are used to model the joints between beams to columns or beams to shear walls. The stiffness of moment-rotation curves is changed in the range from $0.5E_bI_b/L_b$ to $25E_bI_b/L_b$ corresponding to the boundary stiffness of the pinned and rigid connections, respectively, as classified in EC3 [45]. E_b and I_b are the elastic modulus and moment of inertia of the beam, respectively, whilst L_b is the span of the beam.

As can be seen in Fig. 19, the semi-rigid connections have significant effect on both the initial stiffness and the ultimate load-carrying capacity of the composite building. When the stiffness of the connection is increased from $0.5E_bI_b/L_b$ (pinned connection) to $10E_bI_b/L_b$ (semi-rigid connection), a significant improvement in the ultimate base shear force has been observed. However, when the stiffness of the connection exceeds $10E_bI_b/L_b$, the difference in the ultimate base shear force is negligibly small although certain difference in the initial stiffness can be observed.

4.2 Effect of material strength of steel and concrete

In this study, the compressive strength of concrete is varied from 25MPa to 85MPa, whilst the yield stress of steel is taken from 250MPa to 690MPa. In addition, it should be noted that only strengths of materials of columns and shear walls are modified. The effect of the compressive strength of concrete and the yield strength of steel on the load-carrying capacity, drift ratio and lateral displacement of the composite building is illustrated in Fig. 20 for concrete strength and Fig. 21 for steel yield stress. Both figures show that the lateral displacement at each storey and the inter-storey drift ratio increase nonlinearly up to the 30th floor due to large lateral load, and these values increase linearly from the 30th floor upward where the lateral load is smaller.

It can be seen from Fig. 20 that concrete compressive strength has notable effect on the overall behaviour of the composite building. When concrete compressive strength rises, its influence is more evident as the peak points of the base shear force-displacement curves appear at higher concrete strengths and then the base shear force reduces as the concrete becomes crushed. The increase in concrete strength from 25MPa to 85MPa leads to the growth in the ultimate base shear force from 55MN to 75MN, respectively, an increase of approximately 36%. However, this ratio is relatively small when compared with the associated increase of 240% in concrete compressive strength (25MPa to 85MPa). In addition, negligible difference in inter-storey drift ratio and lateral displacement while concrete strength is increased indicates that the compressive strength of in-filled concrete has little contribution to lateral load-carrying capacity of the composite building. The reason for this phenomenon may be the high steel ratio of the structural elements' sections.

The yield strength of steel has demonstrated significant effect on the response of the composite building as depicted in Fig. 21. The ultimate base shear force rises significantly, by approximately 125% (40MN to 90MN), when the steel yield strength is increased by 176% (from 250MPa to 690MPa). In addition, significantly larger displacement and inter-storey drift ratio have been observed when the steel yield strength increases, which indicates that the ductility of the building is also strongly improved.

4.3 Effect of the width-to-thickness ratios of composite shear walls and CFST columns

The width-to-thickness ratios (*B/t*) of composite shear walls and CFST columns are changed in the range from *B/t* = 200 to *B/t* = 25 to investigate their influence on the load-carrying capacity of the composite building. Fig. 22 shows the base shear force – lateral displacement curves of the composite building with various values of B/t ratio. From this figure, it can be concluded that the load-carrying capacity of the building is strongly influenced by the width-to-thickness ratio since the base shear force increased significantly when the *B/t* ratio is changed from 50 to 25. However, with higher values of width-to-thickness ratio (*B/t* = 100 and *B/t* = 200), the difference in the ultimate base shear forces is smaller since other structural elements will contribute more to the overall load-carrying capacity. The co-effect of the width-to-thickness ratios of both shear walls and columns is illustrated in Fig. 22c. It can be seen that the *B/t* ratio of columns has more pronounced effect on the base shear force than that of shear walls. This phenomenon can be explained that the increase of the *B/t* ratio of columns contributes not only to the load-carrying capacity of the building, but also to the overall stiffness of frames, and thus leads to better performance of the composite shear walls as well.

5. Conclusions

This paper investigates the nonlinear behaviour of innovative high-rise composite buildings that comprise of CFST columns and coupling composite shear walls systems by a simple and efficient numerical model proposed by the authors using OpenSees. Since the study focuses on large-scale structure, the slip at concrete-steel interface is ignored. However, through the validation with numerous test data, it is obvious that the modified material constitutive laws and the proposed numerical model capture well the nonlinear behaviour and the loading capacity of composite structures. The failure of these structures is also implicitly predicted but the detail positions of damaged zones cannot be explicitly demonstrated by the beam-column element. Based on the results of the study, some conclusions can be deduced as following:

(1) The stress-strain relationships of materials that are modified based on previous studies can predict the behaviour of CFST members well since the model error is only around 7%. The material models presented in this paper are sufficiently simple and feasible to be applied to practical structures.

(2) The proposed numerical model for composite members, especially the semi-rigid connection and coupling composite shear walls, has shown high accuracy and efficiency. It can predict the nonlinear behaviour, the loading capacity and the failure of the composite structures. Alternatively, the proposed model can also be applied for time history analysis of the composite building, but it is out of scope of the research project.

(3) The case study of 42-story composite building shows that the use of steel-concrete composite structures in the form of CFST sections can increase the strength of building substantially, leading to a significant reduction up to 50% in the sizes required for composite cross-sections compared with the conventional RC cross-sections at the same loading capacity.

(4) The compressive strength of concrete has little influence on the lateral loading capacity of the composite building since the increase of 240% in concrete compressive strength (from 25 MPa to 85 MPa) only leads to 36% increase in the ultimate lateral load of the composite building (from 55 MN to 75 MN). The rise of concrete compressive strength also makes the behaviour of this kind of building more brittle.

(5) The semi-rigid connection has shown great effect on the stiffness and loading capacity of the composite building. Since the stiffness of the semi-rigid connections is increased more than $10E_bI_b/L_b$, the loading capacity of the composite building does not change significantly implying that the governing of the semi-rigid connections is gradually reduced and the yielding of structural members starting to contribute more to the loading capacity of the building.

(6) The yield strength of steel, the width-to-thickness ratio (B/t) of CFST sections and the coupling composite shear walls affect the strength and ductility of the composite building significantly. When the B/t of CFST columns is increased, the stiffness of the whole frame system will also rise leading to better performance of the composite shear walls as well. Hence, the B/t of CFST columns has more pronounced influence on the loading capacity of the building than that of the shear walls.

(7) The proposed model with modified material constitutive laws is efficient with low computational cost. The time for nonlinear simulation of the 42-story building using laptop HP core i7 is under 1 hour, which can never be achieved when using solid or shell elements for this analysis. Therefore, this study can be a benchmark reference for the practical application in the design of such innovative composite buildings.

Acknowledgements

This research was supported by the Australian Research Council (ARC) under its Discovery Scheme (Project No: DP200100112). The financial support is gratefully acknowledged.

References

[1] A. Elremaily and A. Azizinamini, *Journal of Constructional Steel Research* **2002**, *58*, 1567.

[2] L. H. Han, W. D. Wang and X. L. Zhao, *Engineering Structures* **2008**, *30*, 1647.

[3] D. Liu and W. M. Gho, *Thin-Walled Structures* **2005**, *43*, 1131.

[4] Z. Tao, B. Uy, L. H. Han and Z. B. Wang, *Thin-Walled Structures* **2009**, *47*, 1544.

[5] Z. Tao, Z. B. Wang and Q. Yu, *Journal of Constructional Steel Research* **2013**, *89*, 121.

[6] H. T. Thai, B. Uy, M. Khan, Z. Tao and F. Mashiri, *Journal of Constructional Steel Research* **2014**, *102*, 256.

[7] J. Wang, B. Li, D. Wang and C. Zhao, *Engineering Structures* **2017**, *148*, 293.

[8] W. Zhang, K. Wang, Y. Chen and Y. Ding, *Thin-Walled Structures* **2019**, *144*, 106279.

[9] B. Uy, Z. Tao and L. H. Han, *Journal of Constructional Steel Research* **2011**, *67*, 360.

[10] B. Uy, *Journal of Constructional Steel Research* **1998**, *47*, 47.

[11] B. Uy, *Journal of Structural Engineering* **2000**, *126*, 341.

[12] B. Uy, *Journal of Structural Engineering* **2001**, *127*, 666.

[13] B. Uy, *Journal of Constructional Steel Research* **2001**, *57*, 113.

[14] K. Sakino, H. Nakahara, S. Morino and I. Nishiyama, *Journal of Structural Engineering* **2004**, *130*, 180.

[15] T. Fujimoto, A. Mukai, I. Nishiyama and K. Sakino, *Journal of Structural Engineering* **2004**, *130*, 203.

[16] Q. Q. Liang and S. Fragomeni, *Journal of Constructional Steel Research* **2009**, *65*, 2186.

[17] S. Thai, H. T. Thai, B. Uy and T. Ngo, *Journal of Constructional Steel Research* **2019**, *157*, 161.

[18] M. Ozaki, S. Akita, H. Osuga, T. Nakayama and N. Adachi, *Nuclear Engineering and Design* **2004**, *228*, 225.

[19] S. Shafaei, A. Varma, M. Broberg and J. Seo, *Proceedings of the Annual Stability Conference Structural Stability Research Council* **2019**.

[20] A. Varma, M. Bruneau, M. Broberg, S. Shafaei, J. Seo and E. Kizilarslan, *R-Factors for coupled composite plate shear walls / concrete filled (CC-PSW/CF)*, University at Buffalo, **2019**.

[21] C. G. Chiorean, *Engineering Structures* **2013**, *57*, 125.

[22] S. Jeyarajan and J. Y. Richard Liew, *Structures* **2016**, *6*, 20.

[23] J. Nie, M. Tao, C. S. Cai and G. Chen, *Journal of Constructional Steel Research* **2011**, *67*, 1973.

[24] H. T. Thai and B. Uy, *Journal of Constructional Steel Research* **2015**, *112*, 339.

[25] Y. Tang and J. Zhang, *Engineering Structures* **2011**, *33*, 218.

[26] Z. Wang and W. Pan, *Journal of Building Engineering* **2020**, *31*, 101355.

[27] J. Y. R. Liew, H. Chen and N. E. Shanmugam, *Journal of Structural Engineering* **2001**, *127*, 194.

[28] H. T. Thai and S. E. Kim, *Journal of Constructional Steel Research* **2011**, *67*, 585.

[29] H. T. Thai, B. Uy and M. Khan, *Journal of Constructional Steel Research* **2015**, *111*, 57.

[30] V. Terzic, *Force-based element vs. displacement-based element*, UC Berkely, **2011**.

[31] D. C. Kent and R. Park, *Journal of Structural Division* **1971**, *97*, 1969.

[32] ACI318-14, *Building code requirements for strutural concrete*, **2014**.

[33] K. M. A. Farah, *Analytical investigation on non-linear behavior of RC members strengthened with extremely bonded FRP. PhD Thesis*, Department of Engineering and Policy for Sustainable Environment, Hokkaido University, Japan, **2010**.

[34] M. H. M. Yassin, *Nonlinear analysis of prestressed concrete structures under monotonic and cyclic loads. PhD Thesis*, University of California, Berkeley, **1994**.

[35] P. Schneider Stephen, *Journal of Structural Engineering* **1998**, *124*, 1125.

[36] J. B. Mander, M. J. N. Priestley and R. Park, *Journal of Structural Engineering* **1988**, *114*, 1804.

[37] G. G. Balmer, *Shearing strength of concrete under high triaxial stress-computation of Mohr's envelope as a curve*, Denver-Colo. Branch of Design and Construction, **1949**.

[38] F. E. Richart, A. Brandtzaeg and R. L. Brown, *A study of the failure of concrete under combined compressive stresses*, University of Illinois at Urbana Champaign, **1928**.

[39] K. A. S. Susantha, H. Ge and T. Usami, *Engineering Structures* **2001**, *23*, 1331.

[40] J. Tang, S. Hino, I. Kuroda and T. Ohta, *Steel Construction Engineering* **1996**, *3*, 35.

[41] CEB-FIB, *CEB-FIB Model Code: Design Code*, **1993**.

[42] K. Kunnath Sashi, Y. Heo and F. Mohle Jon, *Journal of Structural Engineering* **2009**, *135*, 335.

[43] A. Gomes and J. Appleton, *Engineering Structures* **1997**, *19*, 822.

[44] N. Kishi and W. F. Chen, *Journal of Structural Engineering* **1990**, *116*, 1813.

[45] Eurocode 3, *Design of steel structures-Part 1-8: Design of joints*, **2005**.

[46] Eurocode 4, *Design of composite steel and concrete structures*, **2004**.

[47] Eurocode 2, *Design of concrete structures - Part 1-1 : General rules and rules for buildings*, **2004**.

[48] AISC341-16, *Seismic provisions for structural steel buildings*, **2016**.

[49] J. Nie and C. S. Cai, *Journal of Structural Engineering* **2003**, *129*, 495.

[50] P. Ansourian, *Proc Inst Civ Eng* **1982**, *71(2)*, 25.

[51] AISC360-16, *Specifiation for structural steel buildings*, **2016**.

[52] T. S. Eom, H. G. Park, C. H. Lee, J. H. Kim and I. H. Chang, *Journal of Structural Engineering* **2009**, *135*, 1239.

[53] K. Zhang, A. H. Varma, S. R. Malushte and S. Gallocher, *Nuclear Engineering and Design* **2014**, *269*, 231.

[54] K. Udagawa and H. Mimura, *Journal of Structural Engineering* **1991**, *117*, 1317.

[55] J. F. Wang and G. Q. Li, *Engineering Structures* **2007**, *29*, 1903.

[56] X. Lu, M. Li, H. Guan, X. Lu and L. Ye, *The Structural Design of Tall and Special Buildings* **2015**, *24*.

[57] J. Moehle, Y. Bozorgnia, N. Jayaram, P. Jones, M. Rahnama, N. Shome, Z. Tuna, J. Wallace, T. Yang and F. Zareian, *Case studies of the seismic performance of tall buildings designed by alternative means*, UC Berkely, **2011**.

[58] J. Y. R. Liew, D. X. Xiong and M. H. Zhang, *Proceedings of the 6th Internaltional Symposium on Steel Structures, Seoul, Korea* **2011**, 377.

[59] M. Tomii, *Proceedings of International Colloquium on Stability of Structures Under Static and Dynamic Loads, SSRC/ASCE/Washington, DC* **1977**.

[60] M. D. O'Shea and R. Q. Bridge, *Australian civil engineering transactions* **1998**, *40*, 15.

[61] H. T. Hu, C. S. Huang, M. H. Wu and Y. M. Wu, *Journal of Structural Engineering* **2003**, *129*, 1322.

Table 1. Geometry and ultimate axial load of CFST columns

Specimen	Type	B (mm)	D (mm)	t (mm)	D/t	f_c (MPa)	f_y (MPa)	$P_{u,cal}$ (kN)	$P_{u,exp}$ (kN)	$P_{u,exp}/P_{u,cal}$	Source
SSH-1-2	Rect.	150	150	8	18.8	157	779	7378	6715	0.910	[58]
3MN	Rect.	150	150	3.2	46.9	27.8	300.1	1136	1150	1.012	[59]
UNC-H	Rect.	250	250	2.5	100.0	41.8	338	3345	3200	0.957	[4]
A5-1	Rect.	100	130	5.8	22.4	106	300	1913	1850	0.967	[3]
A6-2	Rect.	170	220	5.8	37.9	83	300	4170	3717	0.891	[3]
A9-1	Rect.	120	120	4	30.0	55	495	1800	1739	0.966	[3]
A14-2	Rect.	100	190	4	47.5	55	495	2150	2138	0.994	[3]
A11-2	Rect.	90	180	4	45.0	55	495	1920	1742	0.907	[3]
CC8-A-8	Cir.	-	108	6.47	16.7	77	853	2525	2713	1.074	[14]
CC4-A-4-1	Cir.	-	149	2.96	50.3	40.5	308	1055	1064	1.009	[14]
CC4-C-4-1	Cir.	-	300	2.96	101.4	41.1	279	3440	3277	0.953	[14]
S16CS80A	Cir.	-	190	1.52	125.0	80.2	306	2482	2600	1.048	[60]
CC4-A-2	Cir.	-	149	2.96	50.3	25.4	308	878	941	1.072	[14]
CC4-A-8	Cir.	-	149	2.96	50.3	77	308	1667	1781	1.068	[14]
CC8-C-4-1	Cir.	-	222	6.47	34.3	40.5	843	5411	5638	1.042	[14]
CU-040	Cir.	-	200	5	40.0	27.15	265.8	1866	2016	1.080	[61]

Note: mean 0.99, standard deviation 0.067

Table 2. Geometry and ultimate lateral load of composite shear walls

Specimen	h (mm)	w (mm)	t (mm)	t_p (mm)	h/w	P (mm)	f_c (MPa)	f_y (MPa)	$V_{u,cal}$ (kN)	$V_{u,exp}$ (kN)	$V_{u,exp}$/ $V_{u,cal}$	Source
DSCW1C	4000	1000	120	10	4.0	-	39.7	383	780	869	1.114	[52]
DSCW3	4000	1000	120	10	4.0	-	39.7	383	1243	1291	1.039	[52]
DSCW4	4000	600	100	5.9	6.7	-	58.7	372	823	835	1.014	[52]
DSCW5	4000	600	100	5.9	6.7	-	58.7	372	1282	1390	1.084	[52]
CW-42-55-10-T	2743.2	924.1	238.3	4.83	3.0	935.0	44.9	422	768	790	1.029	[20]
CW-42-55-20-T	2743.2	924.1	238.3	4.83	3.0	2246.4	53.7	422	891	971.5	1.090	[20]
CW-42-55-30-T	2743.2	924.1	238.3	4.83	3.0	3158.2	50.9	422	924	954.1	1.033	[20]
CW-42-14-20-T	2743.2	924.1	238.3	4.83	3.0	2491.0	60.3	422	861	956.4	1.111	[20]
CW-42-14-20-TS	2743.2	924.1	238.3	4.83	3.0	2402.0	58.0	422	850	938.6	1.104	[20]

Note: mean 1.069, standard deviation 0.04

Table 3. Sections and material properties of structural elements in 42-storey composite building

Structural elements		Dimensions (mm)	Material properties	
			f_c (MPa)	f_y (MPa)
Composite beams	RC slab Steel beam	1200x200 700x500x12x25	45	450
CFST columns		600x600x12	45	450
Composite shear walls		350x7	45	450

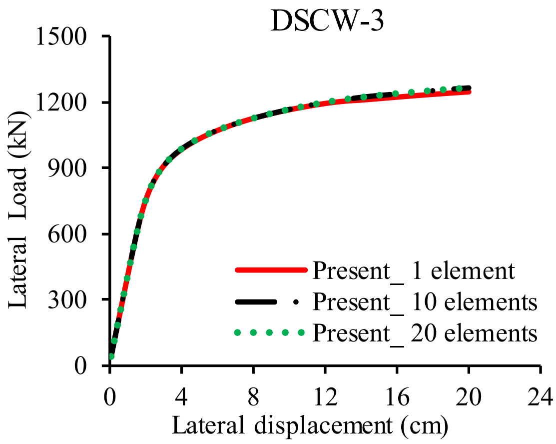

Fig. 1. The effect of mesh sensitivity on load-displacement curve of shear wall DSCW-3

(a) Model for concrete (b) Model for steel

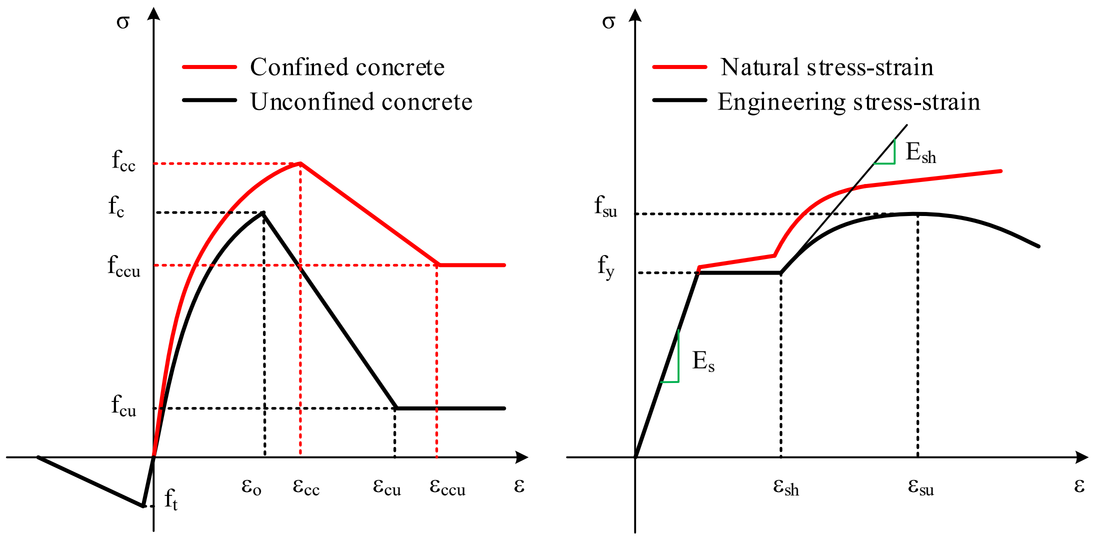

Fig. 2. Material models for concrete and steel

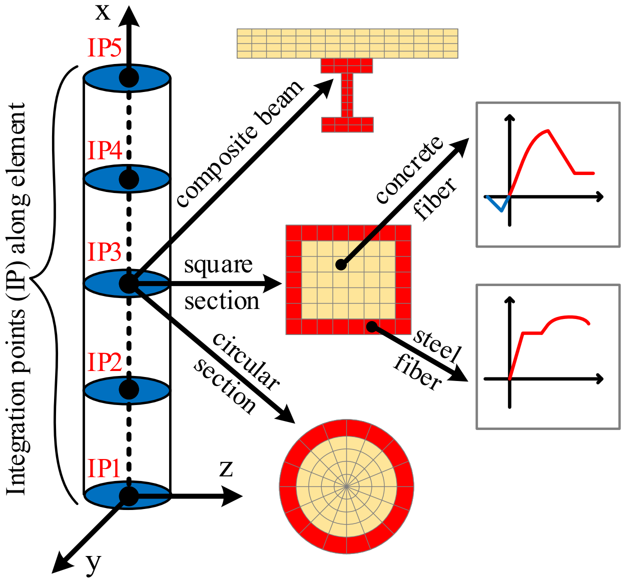

Fig. 3. Beam-column element with fibre sections

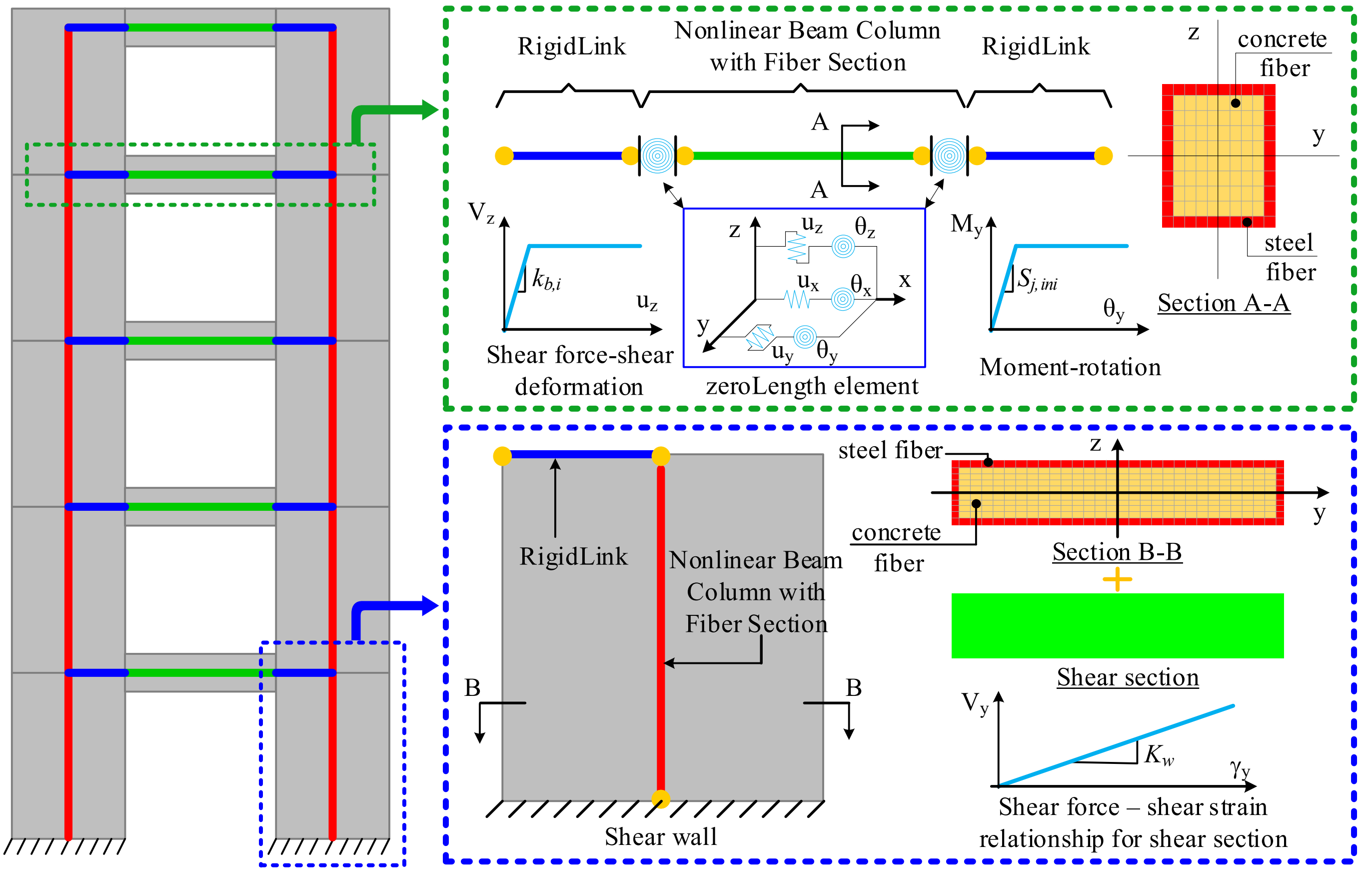

Fig. 4. Model for coupling shear walls

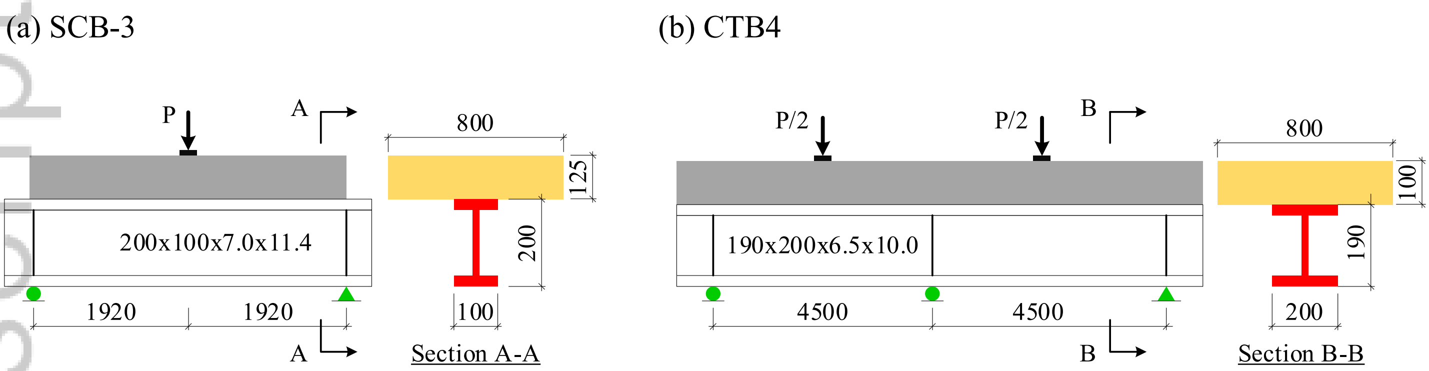

Fig. 5. Geometry of composite beams (Unit: mm)

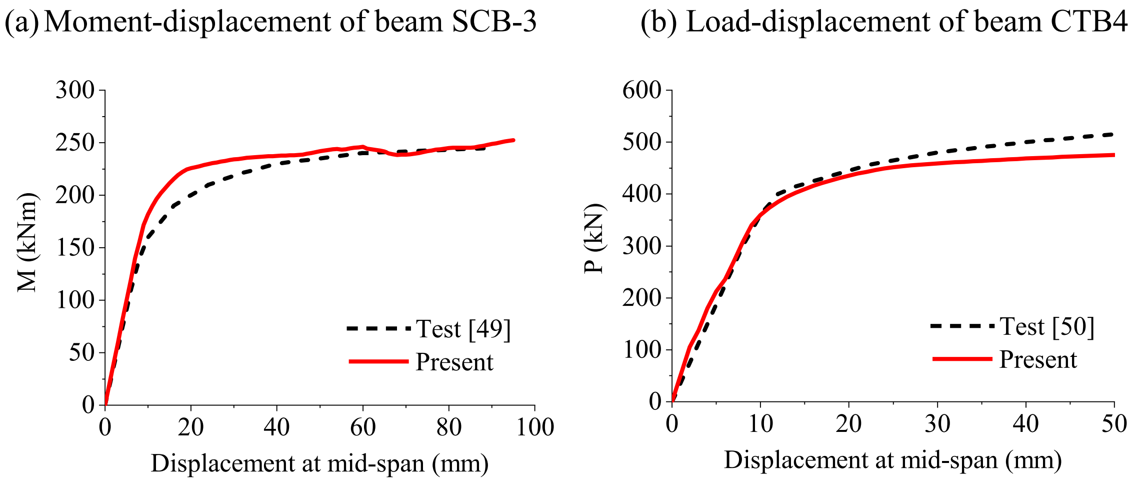

Fig. 6. Comparison on results of composite beams

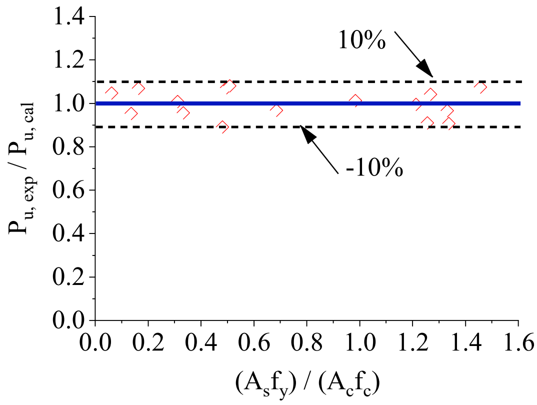

Fig. 7. Comparison on the ultimate load of CFST columns

(a) SSH-1-2

(b) 3MN

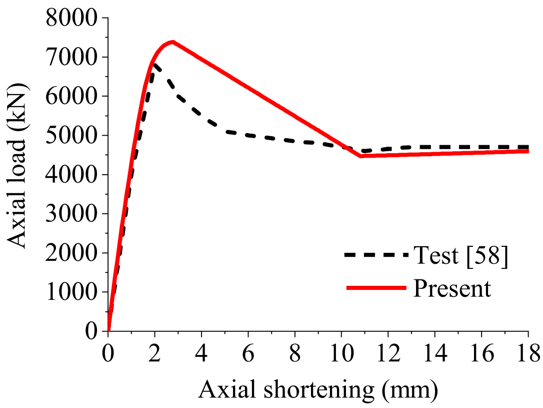

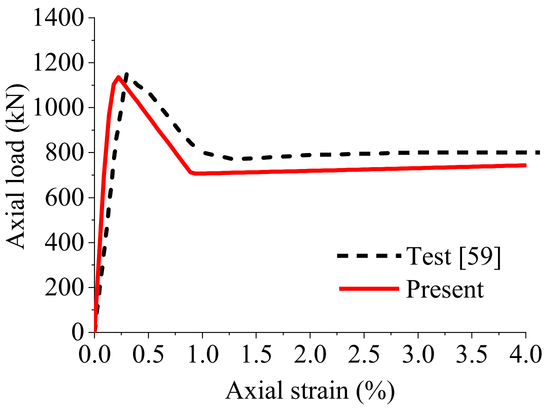

(c) UNC-H

(d) A5-1

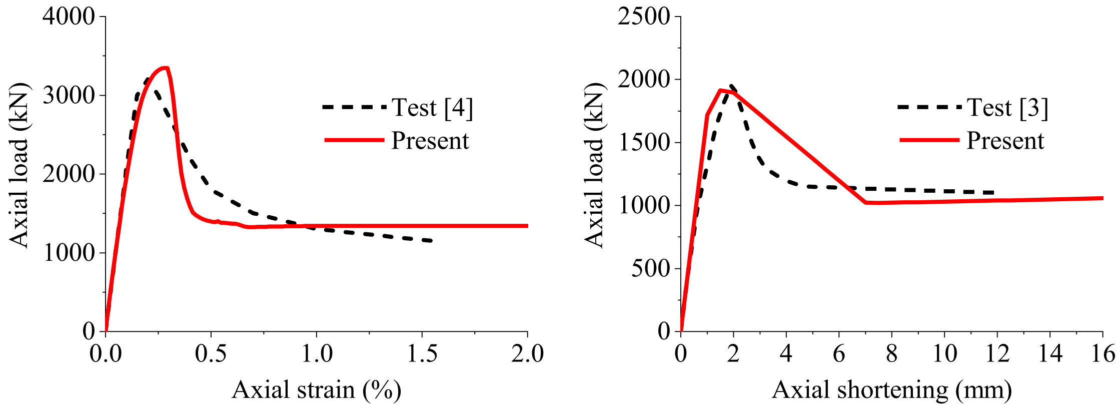

Fig. 8. Comparison on the load-deformation curves of rectangular CFST columns

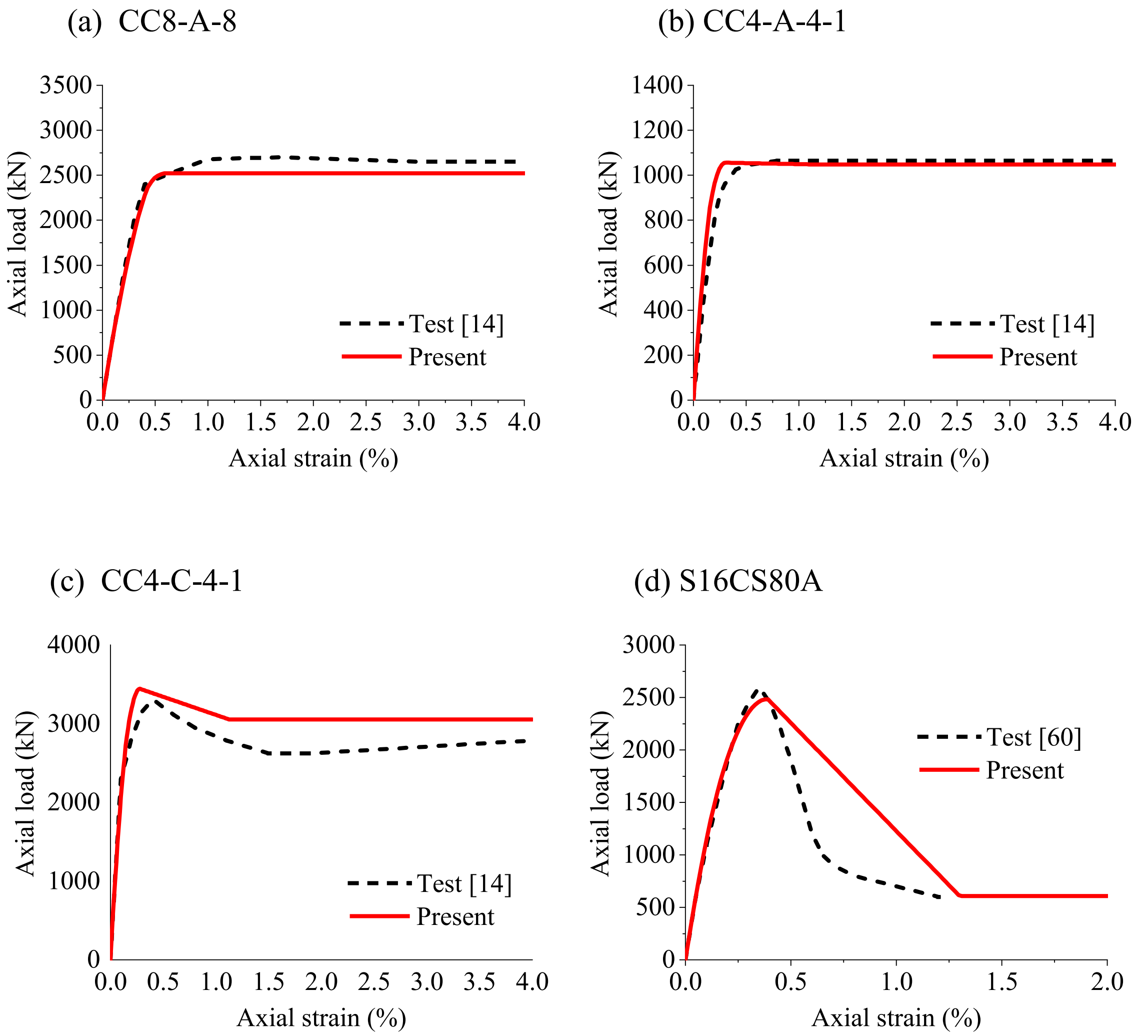

Fig. 9. Comparison on the load-deformation curves of circular CFST columns

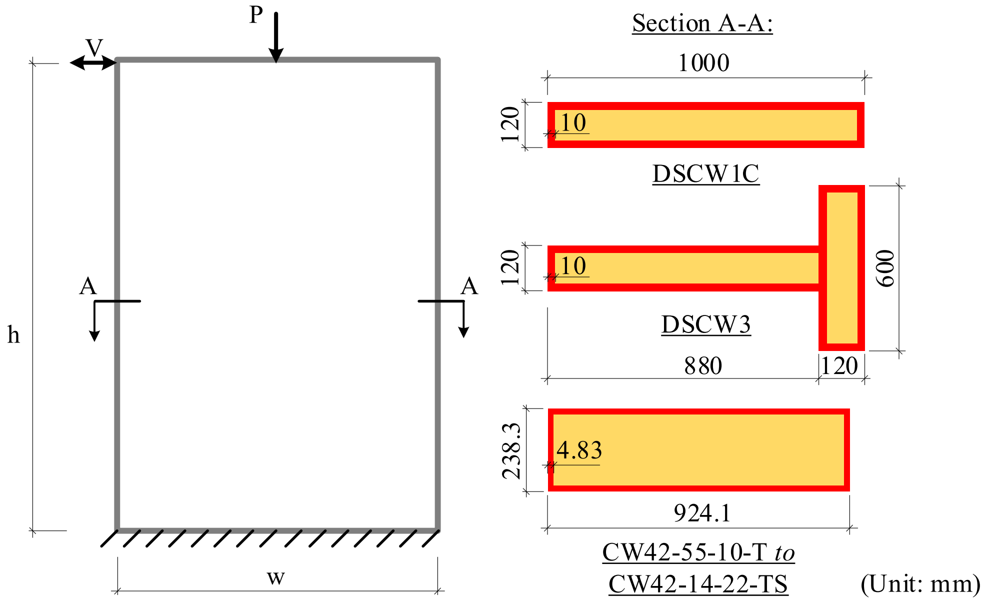

Fig. 10. Geometry of isolated composite shear walls

(a) DSCW1C

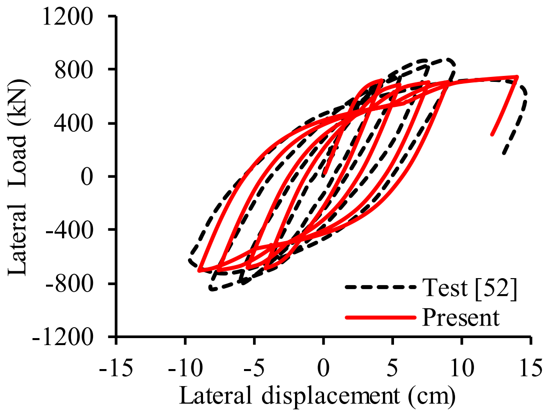

(b) DSCW3

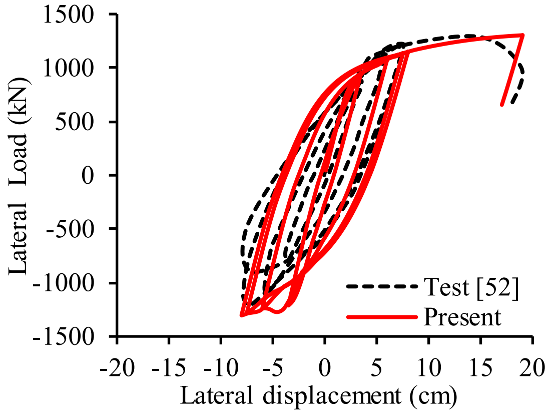

(c) CW-42-55-10-T

(d) CW-42-55-30-T

(e) CW-42-55-20-T

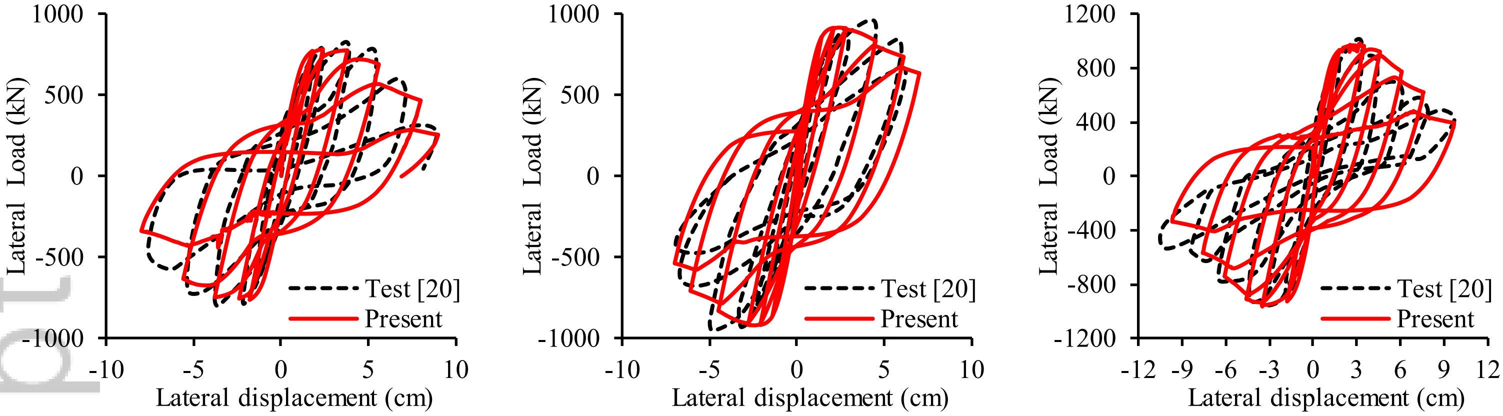

(f) CW-42-14-20-T

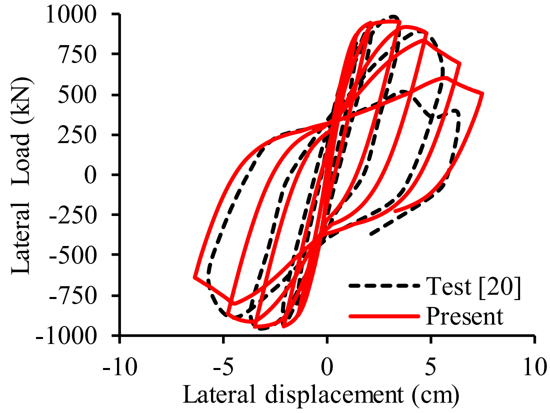

(g) CW-42-14-20-TS

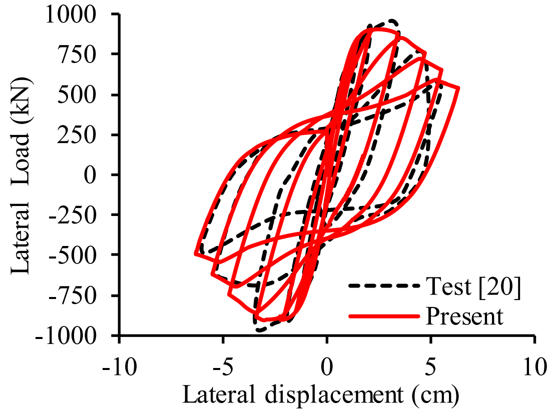

Fig. 11. Comparison on the load-displacement backbone curves of composite shear walls

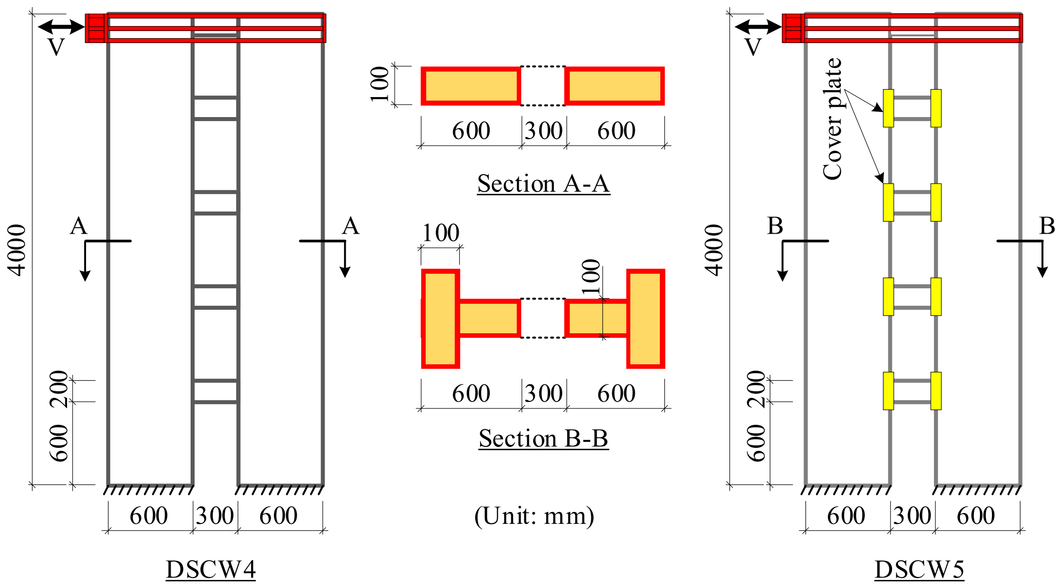

Fig. 12. Geometry of coupling composite shear walls

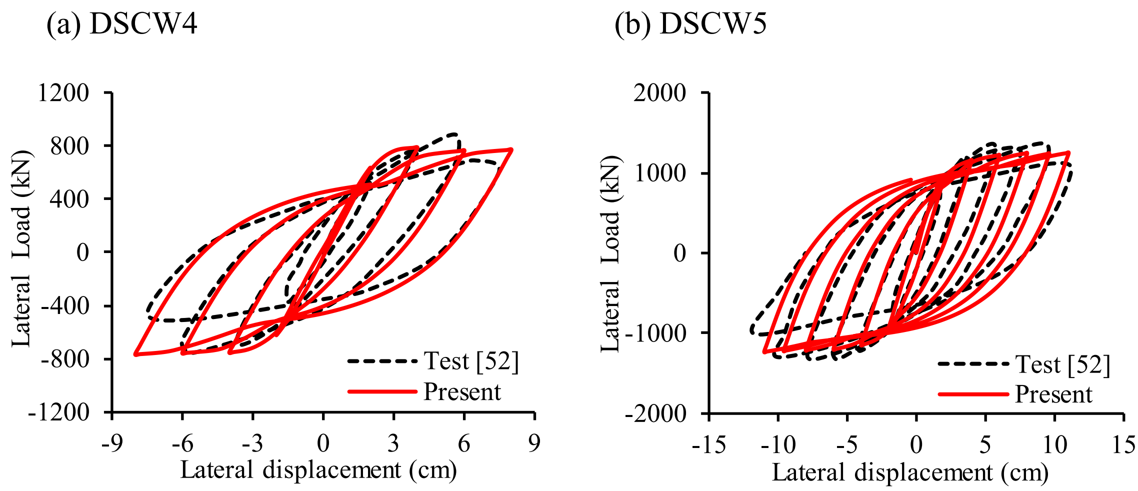

Fig. 13. Comparison on the load-displacement curves of coupling composite shear walls

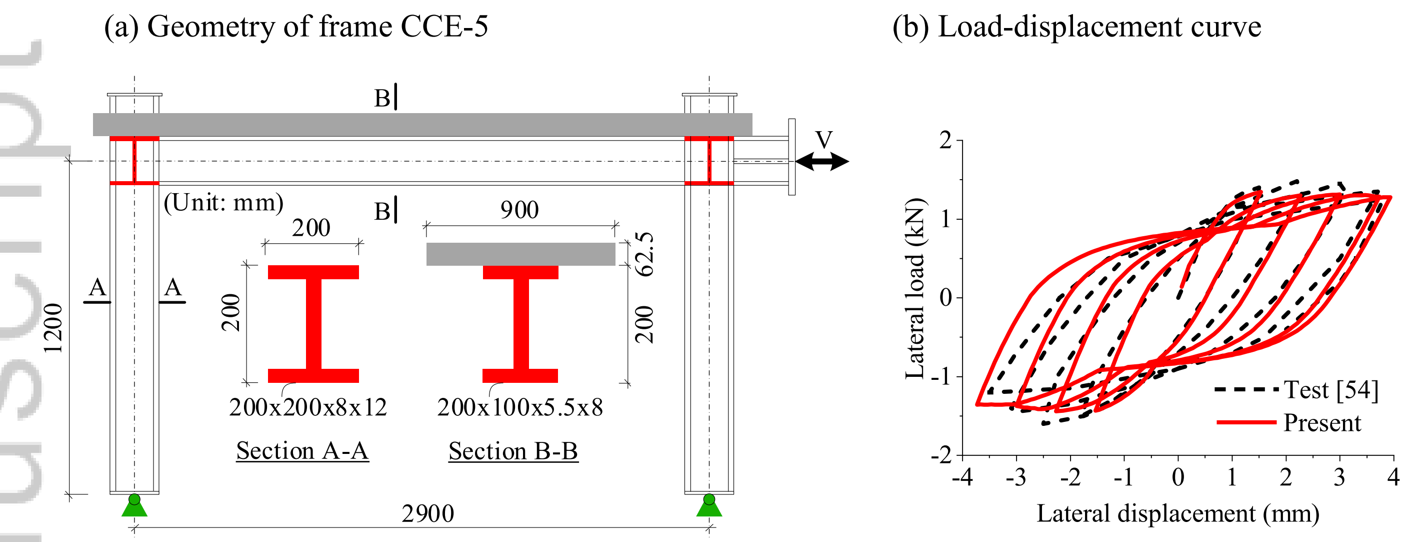

Fig. 14. Frame with steel columns and composite beam

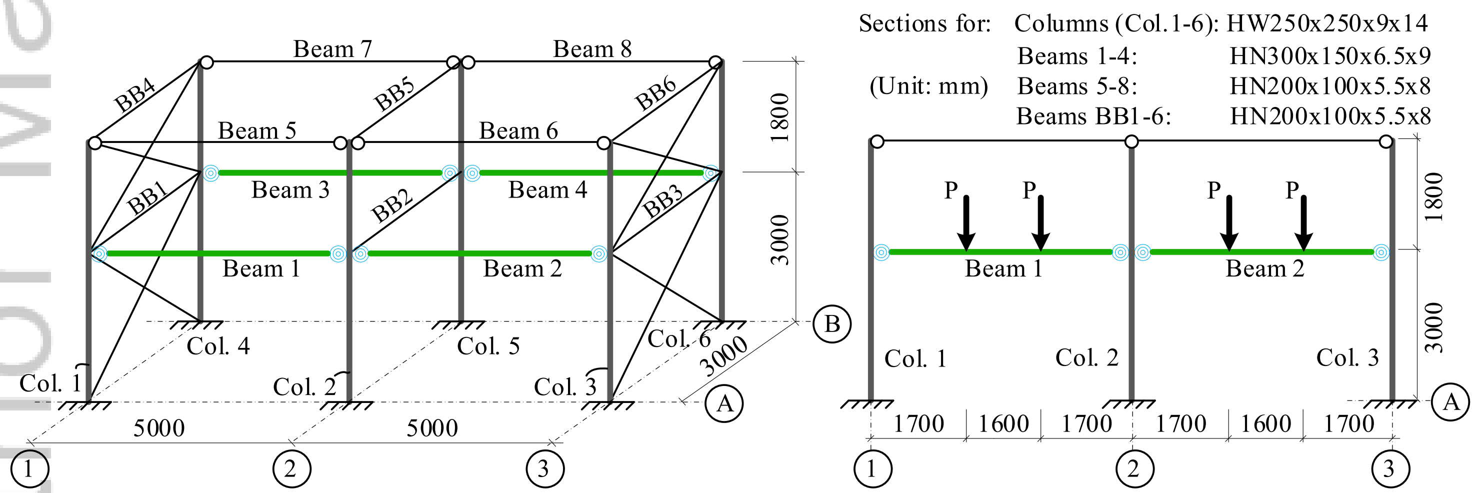

Fig. 15. Two-storey two-bay composite frame

(a) Load-mid span displacement curve (b) Moment distribution

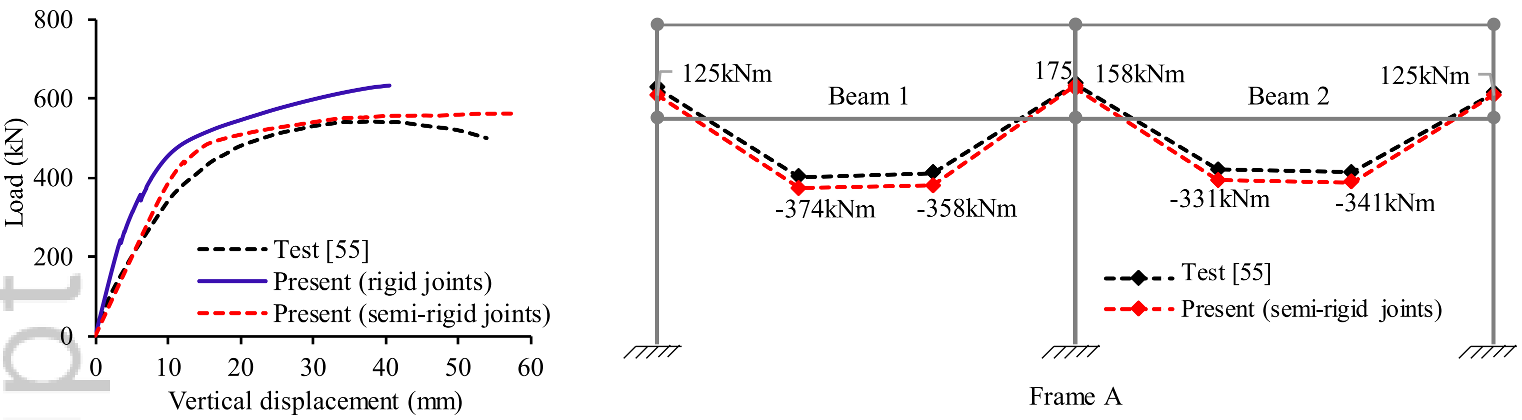

Fig. 16. Comparison of the two-storey two-bay composite frame

(a) Composite building in the present study (b) RC building (building 2A) modelled in [56]

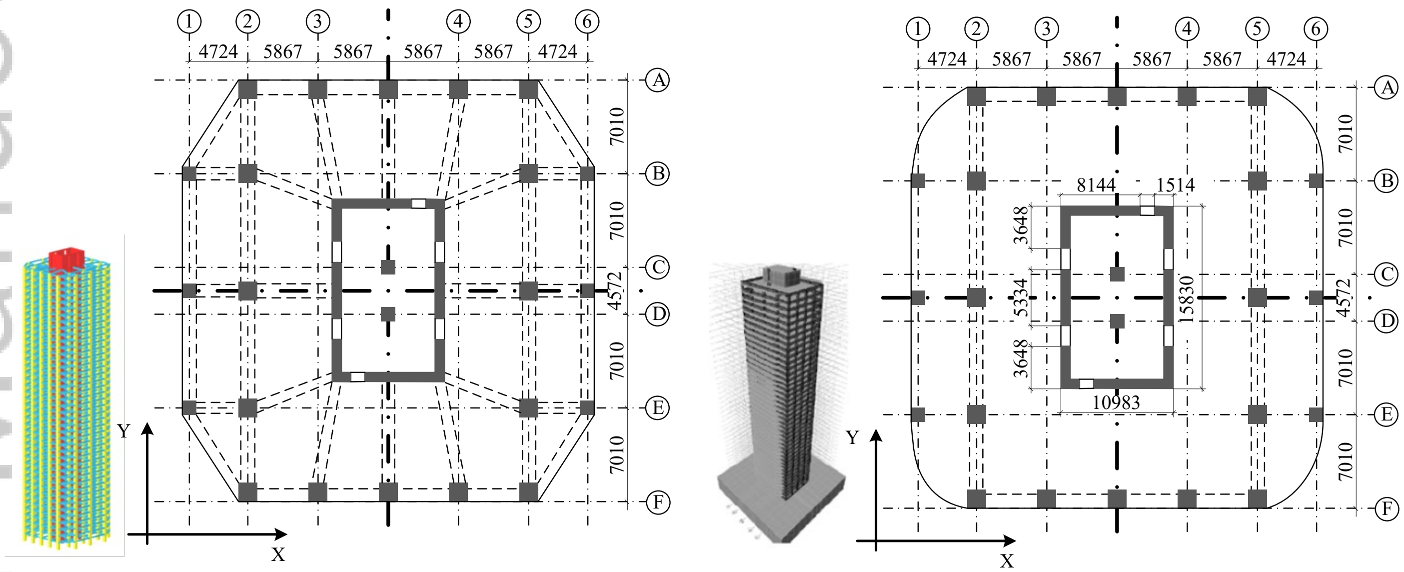

Fig. 17. 3D view and plan of 42-storey buildings.

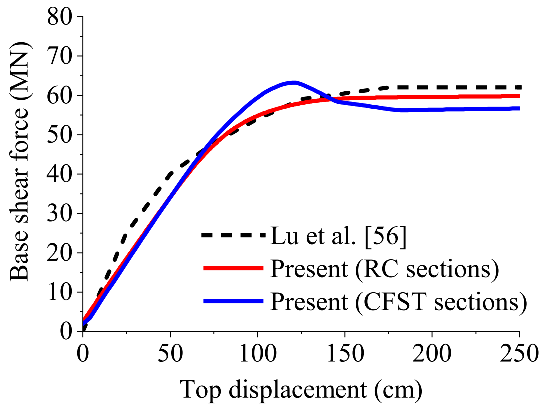

Fig. 18. Results of pushover analysis

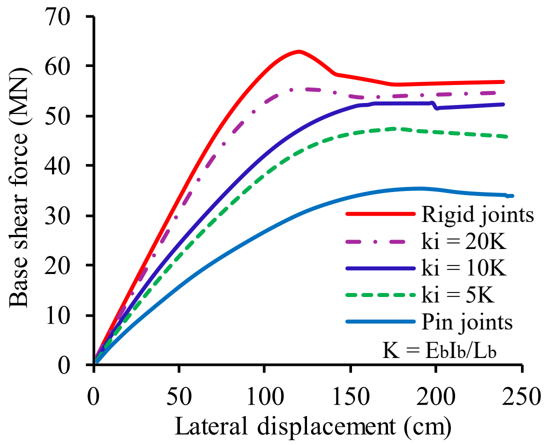

Fig. 19. The effect of the semi-rigid connections

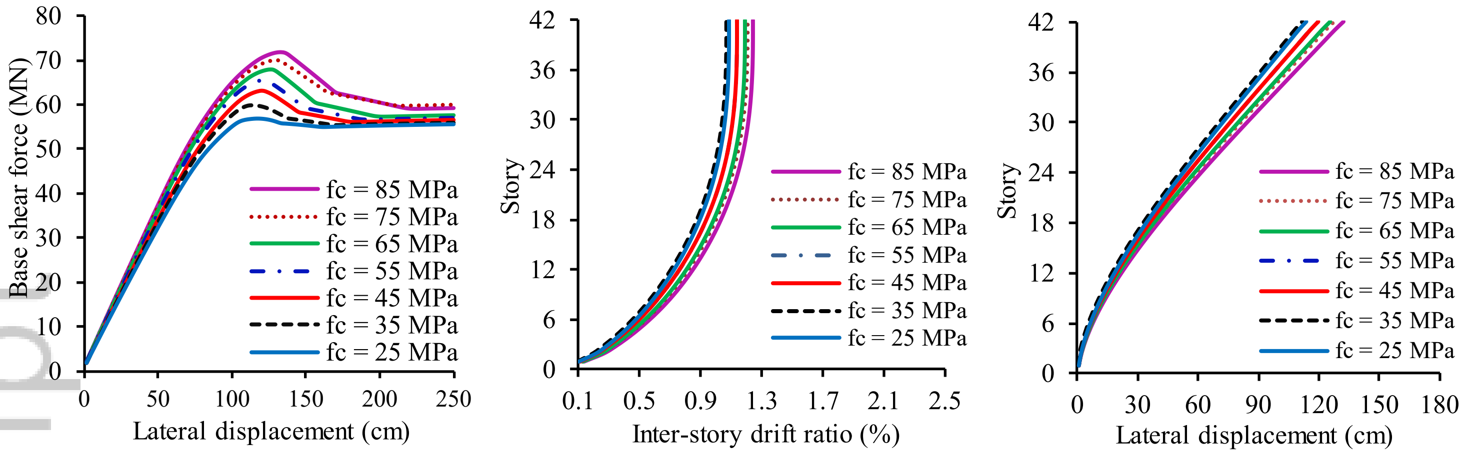

Fig. 20. The effect of the concrete compressive strength

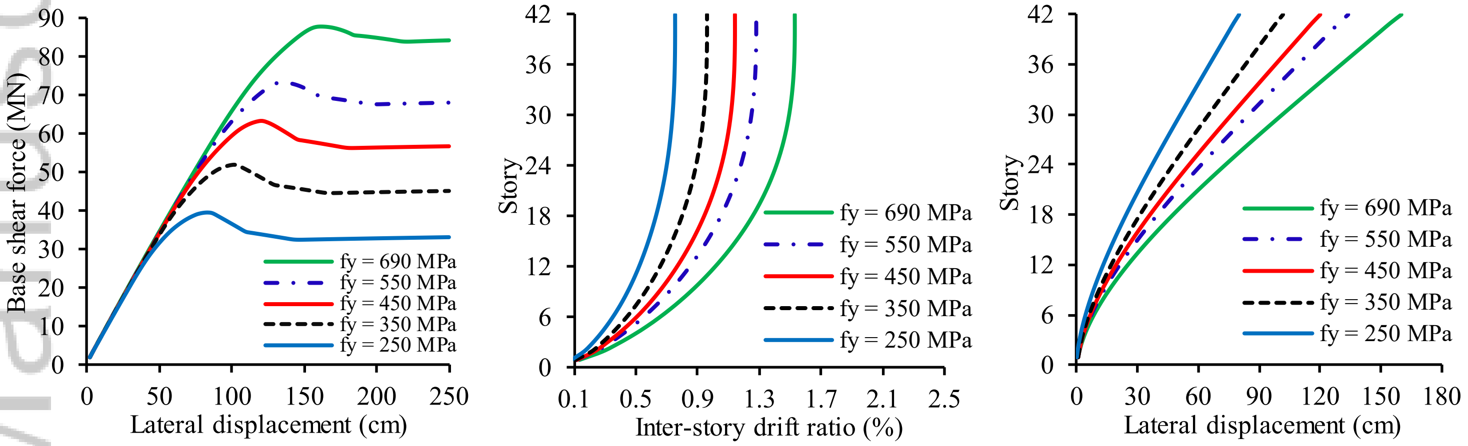

Fig. 21. The effect of the steel yield strength

(a) B/t of composite shear walls (b) B/t of CFST columns (c) B/t effect of both columns and shear walls

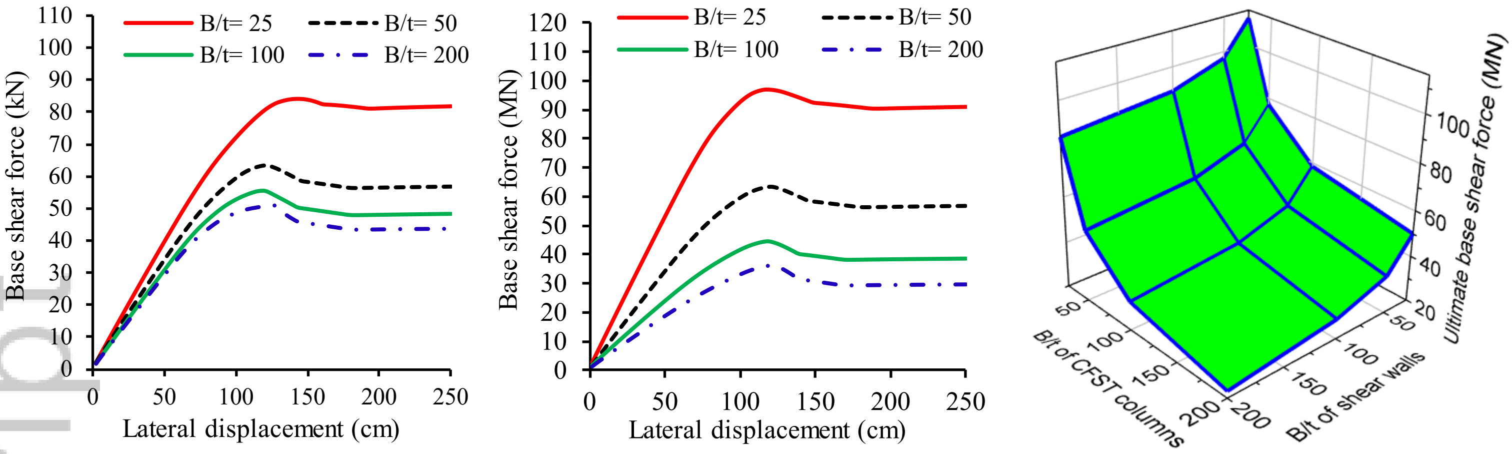

Fig. 22. The effect of the width-to-thickness ratio of shear walls and CFST columns